IMPROVED MESH SEQUENCING METHOD FOR THE ACCELERATED SOLUTION OF THE COMPRESSIBLE EULER AND NAVIER-STOKES EQUATIONS

D.Drikakis* and S.Tsangaris**
Laboratory of Aerodynamics
National Technical University of Athens
Greece

Abstract

The solution of the compressible Euler and Navier - Stokes equations via an upwind finite volume scheme is obtained. For the inviscid fluxes the monotone, upstream centered scheme for conservation laws (MUSCL) has been incorporated into a Riemann solver. The flux vector splitting method of Steger and Warming is used with some modifications. The MUSCL scheme is used for the unfactored implicit equations which are solved by a Newton form and relaxation is performed with a Gauss-Seidel technique. The solution on the fine grid is obtained by iterating first on a sequence of coarse grids and then interpolating the solution up to the next refined grid.

Because the distribution of the numerical error is not uniform, the local solution of the equations in regions where the numerical error is large can be obtained.

The choice of the partial meshes, in which the iterations will be continued, is determined by the use of an adaptive procedure taking into account some convergence criteria.
Reduction of the iterations for the two dimensional problem is obtained via the local adaptive mesh solution which is expected to be more effective in three dimensional complex flow computations.

Introduction

During the last decade a wide variedy of numerical methods for the solution of the Euler and the Navier - Stokes equations has been developed. Most of these schemes make use of the eigenvalues and eigenvectors that belong to the coefficient matrices of the Euler equations. These methods find the sign of the eigenvalues and make use of this information for the discretization of the equations. In the recent past many upwind shock capturing schemes for the computation of the Euler equations have been presented[1,2,5,6,7]

Most of these methods are very different in form but all of these can yield accurate results even though no grid refinements and no control of any parameter have been used. Details for the formulation of such approaches can be found in the literature and some of these are reported in Refs: 2, 4,5,6. In this paper the monotone upstream centered scheme for conservation laws[7](MUSCL) has been used for the calculation of the conservative variables at the cell faces. This upwind scheme has been incorporated into a very robust, locally one dimensional Riemann solver [8]. The above method is used for the calculation of the inviscid fluxes. Another known approach for the calculation of the inviscid fluxes is the flux vector splitting method[6],which makes use of the homogeneity property of the Euler equations. In this approach the fluxes are split into backward and forward contributions by splitting the eigenvalues of the Jacobian matrix of the flux into positive and negative parts. The split fluxes are then differenced regarding upwind discretizations. In the present paper second order accuracy is used for the definition of the left and right states at the cell faces, in conjuction with the flux vector splitting. Validations of the flux vector splitting methods have been reported in the past[10].

In this paper a modified flux vector splitting with second order spatial accuracy and the MUSCL scheme in conjuction with the Riemann solver are used.

An upwind scheme is also used for the calculation of the viscous terms[9].

The numerical solution, either for the Euler or for the Navier - Stokes equations, is obtained after a number of iterations. Many implicit methods use the unfactored equations and find the solution to the steady state using a Gauss-Seidel relaxation technique[3,4,9]. The present method is an implicit relaxation scheme which allows high CFL numbers.
Inspite of these techniques the cost for the solution of the Navier - Stokes or the Euler equations is high. Thus, many times the calculation of complicated flows is impractical in a design environment. On the other hand, the flows are nonuniform concerning the gradients[12]. Nonuniformities are especially present near the boundaries and in shock waves. Therefore, a large part of the flow field has converged during the iterations while more time steps are needed for "strong" regions where the convergence criteria are not satisfied.

In this paper the solution of the equations is obtained at first on a sequence of coarser grids and then interpolating the solution up to the next finer grid. After the smoothness of the solution on the finest grid and using prescribed convergense criteria, blocks of the grid are choosen for the local solution of the equations. The adaptation of the partial grid distribution is obtained using some convergence criteria and an optimum number of grid points which are needed for the local solution.

The above method is expected to be more effective for complex calculations in meshes with a large number of grid points,(i.e 3D flow)in which the points of the partial meshes will be a smaller fraction of the whole grid, than for the two dimensional problem.

Governing Equations and time integration

The governing equations are the time dependent Navier - Stokes equations. These equations

* Ph.D student
** Assistant Professor

can be written in conservation form and for a generalized coardinate system as:

$$U_t + (E_{inv})_\xi + (G_{inv})_\zeta = (E_{vis})_\xi + (G_{vis})_\zeta$$

$$U = J.\ (\rho, \rho u,\ \rho w,\ e)^T \qquad (1)$$

where

$$E_{inv} = J(\tilde{E}\xi_x + \tilde{G}\xi_z)$$

$$G_{inv} = J\ (\tilde{E}\zeta_x + \tilde{G}\zeta_z)$$

$$E_{vis}\ J\ (\tilde{R}\xi_x + \tilde{S}\xi_z)$$

$$G_{vis} = J(\ \tilde{R}\zeta_x + \tilde{S}\zeta_z)$$

$\tilde{E},\tilde{G},\tilde{R},\tilde{S}$ are the Cartesian fluxes:

$$\tilde{E} = \begin{bmatrix} \rho u \\ \rho u^2 + p \\ \rho uw \\ (e+p)u \end{bmatrix}$$

$$\tilde{G} = \begin{bmatrix} \rho w \\ \rho uw \\ \rho w^2 + p \\ (e+p)w \end{bmatrix}$$

$$\tilde{R} = \begin{bmatrix} 0 \\ \tau_{xx} \\ \tau_{xz} \\ u\tau_{xx} + w\tau_{xz} - q_x \end{bmatrix}$$

$$\tilde{S} = \begin{bmatrix} 0 \\ \tau_{zx} \\ \tau_{zz} \\ u\tau_{xz} + w\tau_{zz} - q_z \end{bmatrix}$$

The Euler equations are obtained from the above equations by eliminating the viscous flux vectors $\tilde{R},\tilde{S}$ and retaining the inviscid flux vectors $\tilde{E},\tilde{G}$. Body fitted arbitrary coordinates ξ,ζ are used. The Jacobian of the transformation $\xi=\xi(x,z), \zeta=\zeta(x,z)$ from Cartesian coordinates x,z to generalized coordinates is written as:

$$J = x_\xi z_\zeta - z_\xi x_\zeta$$

The quantities ρ,p,u,w,e represent the density the pressure and the cartesian velocity components and the total energy respectively. The viscous stresses are:

$$\tau_{xx} = -p - \frac{2}{3}\mu\ (-2u_x + w_z)$$

$$\tau_{zz} = -p - \frac{2}{3}\mu(u_x - 2w_z)$$

$$\tau_{xz} = \tau_{zx} = \mu(w_x + u_z)$$

and the heat flux vector:

$$q_x = -\kappa T_x\ ,\quad q_z = -\kappa T_z$$

μ,K are the viscosity and heat conductivity coefficient and T the temperature. The indices $(\ )_\xi$, $(\ )_\zeta, (\ )_x, (\ )_z$ denote partial derivatives with respect to ξ,ζ,x,z except for the stresses and the heat flux vector.
The formulation of the governing equations is completed by the perfect gas equation of state.

$$p = (\gamma - 1)\rho i$$

where i is the internal energy and γ is the ratio of the specific heat capacities of the fluid.
To reach the steady state solution asympotically, an implicit procedure is used which allows high CFL numbers [3][9][4]. The first order in time, discretized, implicit form of eq. (1) is written as:

$$\frac{U^{n+1} - U^n}{\Delta t} + E_\xi^{n+1} + G_\zeta^{n+1} = 0 \qquad (2)$$

where $E = E_{inv} + E_{vis}$

$G = G_{inv} + G_{vis}$

A Newton method can be constructed for U^{n+1} by linearizing the fluxes in eq. (2) about the known time level n.

$$E^{n+1} = E^n + A^n.\Delta U$$
$$G^{n+1} = E^n + C^n.\Delta U$$

The last relations yield the eq.(2) to the following form:

$$\frac{\Delta U}{\Delta t} + (A^n.\Delta U)_\xi + (C^n.\Delta U)_\zeta = -(E_\xi^n + G_\zeta^n) = RHS \qquad (3)$$

A,C are the Jacobians of the flux vectors E,G :

$$A = \frac{\partial E}{\partial U}\ ,\ C = \frac{\partial G}{\partial U}$$

ΔU is the time variation of the solution:

$$\Delta U = U^{n+1} - U^n$$

The terms $(A^n\Delta U)_\xi$, $(C^n.\Delta U)_\zeta$ are discretized[3][4] at the volume (i.k) up to second order accuracy in space. For example the term $(A^n\Delta U)_\xi$ is written as:

$$(A^n\Delta U)_\xi = (A^n_{inv}.\Delta U)_{i+\frac{1}{2}} - (A^n.\Delta U)_{i-\frac{1}{2}} + (A^n_{vis})_i .$$

$$(\Delta U_{i+1} - 2\Delta U_i + \Delta U_{i-1})$$

where

$$(A^n\Delta U)_{i+\frac{1}{2}} = (T\Lambda^+T^{-1})_{i+\frac{1}{2}}.\Delta U^+_{i+\frac{1}{2}} + (T\Lambda^-T^{-1})_{i+\frac{1}{2}}\Delta U^-_{i+\frac{1}{2}}$$

$$(A^n.\Delta U)_{i-\frac{1}{2}} = (T\Lambda^+T^{-1})_{i-\frac{1}{2}}.\Delta U^+_{i-\frac{1}{2}} + (T\Lambda^-T^{-1}).\Delta U^-_{i-\frac{1}{2}}$$

Λ^+, Λ^- are the diagonal matrices of the positive and the negative eigenvalues of the Jacobian A, respectively. The above matrices are defined as follows:

$$\Lambda^+ = \max(0,\Lambda),\ \Lambda^- = \min(0,\Lambda)$$

where Λ is the diagonal eigenvalue matrix:

$$\Lambda = \mathrm{diag}(\ \lambda^0_K\ ,\ \lambda^0_K\ ,\ \lambda^1_K\ ,\ \lambda^2_K\ )$$

with elements

$$\lambda^0_\kappa = u\,\kappa_x + w\kappa_z$$

$$\lambda^1_\kappa = \lambda^0_\kappa + S|\nabla\kappa|$$

$$\lambda^2_\kappa = \lambda^0_\kappa - S|\nabla\kappa|$$

The above elements define the eigenvalues of the matrix A,C for $\kappa=\xi$, $\kappa=\zeta$ respectively. The vectors ΔU are extrapolated consistently on the right hand side. For the finite volume face $(i+\frac{1}{2},\kappa)$, ΔU is extrapolated up to second order depending on the eigenvalues. Γ,Γ^{-1} are the matrices of the left and the right eigenvectors, respectively. The solution of the system of equations (3) is obtained by a sequence of approximations denoted by q^v such that $\lim q^v \to U^{n+1}$ where $v>1$ is the subiteration state. The equations are solved by a Newton method[4] [9]. The Newton form is obtained by the linearization of the equation (3) around the known subiteration state v, as follows:

$$\frac{\Delta q^{v+1}}{\Delta t} + (A^v.\Delta q^{v+1})_\xi + (C^v.\Delta q^{v+1})_\zeta = \frac{U^n - q^v}{\Delta t}$$

$$- (E^v_\xi + G^v_\zeta) = RHS$$

q^v, q^{v+1} are the solution vectors at the subiteration states v,v+1 respectively. The solution at the level v+1 is updated as:

$$q^{v+1} = q^v + \Delta q^{v+1}$$

Inviscid fluxes

MUSCL approach

For the inviscid fluxes on the RHS of equation (3) a linear, locally one-dimensional Riemann solver (Godunov type differencing) is employed at the finite volume cell faces. The state which is used for the Riemann solution depends on the sign and the size of the eigenvalues[2] [8]. A mean value is obtained at the cell faces as follows:

$$U_{i+\frac{1}{2}} = \frac{1}{2}\left[(1+\xi_j)\,U_l + (1-\xi_j)\,U_r\right]$$

The index j denote the number of the eigenvalue (0,1,2). The term ξ_j is defined as

$$\xi_j = \left[\frac{\lambda_l + \lambda_r}{|\lambda_l| + |\lambda_r|}\right]_j$$

The left (l) and the right (r) conserved state variables are obtained by an upwind-biased interpolation [7] [10] which is known as MUSCL type approach.
A general MUSCL - type scheme can be defined as

$$(U_l)_{i+\frac{1}{2}} = U_i + \frac{S}{4}\left((1-KS)\nabla_\xi + (1+KS)\Delta_\xi\right)U_i$$

$$(U_r)_{i+\frac{1}{2}} = U_{i+1} - \frac{S}{4}\left((1-KS)\Delta_\xi + (1+KS)\nabla_\xi\right)U_{i+1}$$

The symbols Δ and ∇ denote the forward and the backward difference operators:

$$\Delta_\xi U_i = U_{i+1} - U_i$$

$$\nabla_\xi U_i = U_i - U_{i-1}$$

S is the van Albada type sensor [7] for the detection of shocks and other discontinuities

$$S = \frac{2\Delta_\xi.\nabla_\xi}{(\Delta\xi)^2 + (\nabla\xi)^2 + \varepsilon}$$

where ε is a small number to prevent division by zero. Such limiters as the above, called flux limiters, originate from the theory of almost monotonic solutions (TVD methods) and are applied to hyperbolic systems in multi-dimensions. The parameter K defines the spatial accuracy of the approximation. K=-1 corresponds to the fully upwind second order scheme and K=1/3 to the third order biased scheme.

The above MUSCL-type interpolation was incorporated into the Riemann solver[4] for the evaluation of the conservative variables at the cell faces.

Flux vector splitting

The flux vector splitting method[6] is used as a second approximation for the inviscid fluxes.

The fluxes are split into negative and positive parts in accordance with the eigenvalue sign. The inviscid flux vector E_{inv} at the cell face is written as:

$$(E_{inv})_{i+\frac{1}{2}} = E^+(U^-_{i+\frac{1}{2}}) + E^-(U^+_{i+\frac{1}{2}}) =$$
$$(T\Lambda^+T^{-1})\,U^-_{i+\frac{1}{2}} + (T\Lambda^-T^{-1})U^+_{i+\frac{1}{2}}$$

The splitting of the fluxes is made in accordance with the eigenvalues λ_1 , λ_2. The splitted eigenvalues are defined as:

$$\lambda^\pm_o = \frac{1}{2}\left(\lambda^\pm_1 + \lambda^\pm_2\right)$$

$$\lambda^\pm_1 = \frac{1}{2}\left(\lambda_1 \pm |\lambda_1|\right)$$

$$\lambda^\pm_2 = \frac{1}{2}\left(\lambda_2 \pm |\lambda_2|\right)$$

The flux vectors $E^\pm_{inv}$, $G^\pm_{inv}$ are given as

$$E^\pm, G^\pm = \begin{bmatrix} \frac{\rho}{2}\left(\lambda^\pm_1 + \lambda^\pm_2\right) \\ \left(u+S\frac{K_x}{\nu|\nabla\kappa|}\right)\frac{\rho}{2}\lambda^\pm_3 + \left(u-S\frac{K_x}{\nu|\nabla\kappa|}\right)\frac{\rho}{2}\lambda^\pm_4 \\ \left(w+S\frac{K_z}{\nu|\nabla\kappa|}\right)\frac{\rho}{2}\lambda^\pm_3 + \left(w-S\frac{K_z}{\nu|\nabla\kappa|}\right)\frac{\rho}{2}\lambda^\pm_4 \\ H^\pm.\frac{\rho}{2}\left(\lambda^\pm_3 + \lambda^\pm_4\right) \end{bmatrix}$$

where H,S is the total enthalpy and the speed of sound respectively and $\kappa=\xi,\zeta$.
The variables $U^-_{i+\frac{1}{2}}$, $U^+_{i+\frac{1}{2}}$ are defined for second order spatial accuracy as:

$$U^-_{i+\frac{1}{2}} = U_i + 0.5\,(U_i - U_{i-1})$$

$$U^+_{i+\frac{1}{2}} = U_{i+1} + 0.5\,(U_{i+1} - U_{i+2})$$

Transonic flow over circular arc -airfoil

The inviscid flow over a circular arc-airfoil with thickness 10% is studied using the above two methods for the discretization of the inviscid fluxes. The free stream Mach number is 0.85 and the angle of attack zero. For sipplicity the half computational plane is considered, with symmetry conditions on the upstream and on the downstream side along the x-axis. Initially are shown the experi-

ments on a coarse grid 54X25(fig.1). For all the above test cases no grid refinement has been used near the shock region. In figure 2a, 2b the Mach number distribution is shown for the flux vector splitting and the Riemann solver with the MUSCL type scheme respectively. From this figure is shown that the sharpness of the shock is better with the MUSCL upwind into the Riemann solver. The pressure coefficient distribution is presented in figure 3. It is noted that no blending term[6] [10] was added to the eigenvalues in the flux vector splitting approach.

In order to examine the grid dependence of the Riemann solver with MUSCL upwind two finer grids have been used, without clustering in the shock region. The first is a 64X25 mesh and the second a 96X35 mesh. In figure 4 the pressure coefficient distribution is compared for the two finer grids 64X25 and 96X35 respectively. From these comparisons it is shown that with the MUSCL upwind,incorporated into the Riemann solver, accurate results can be obtained without very fine meshes. Finally in figure 5 the isomach lines are plotted for the finest mesh 96X35. The last approach is used in the next paragraphs for the local adaptive solution of the Euler and the Navier - Stokes equations.

Viscous terms

The viscous terms are discretized using central differences for the $\xi,\zeta=$ const cell faces and an upwind discretization for the cross derivatives terms,which have been proposed by Chakravarthy[9] et al, is applied. Similar treatment has used by Schmatz[4]. Because fictitious mesh points are needed for boundary cells,simple linear extrapolation is used for the evaluation of these points.

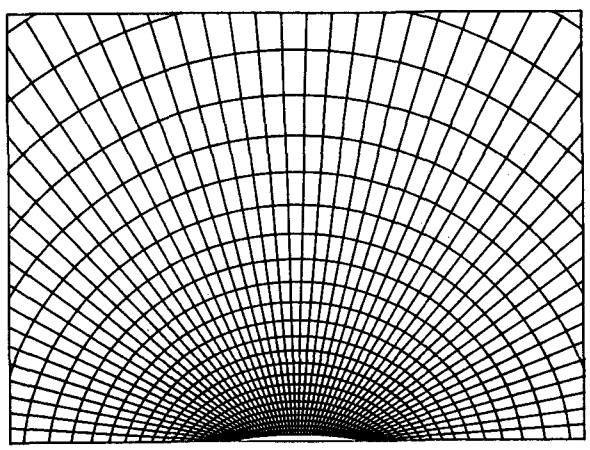

Fig.1: Mesh (54X25) around the circular arc-airfoil

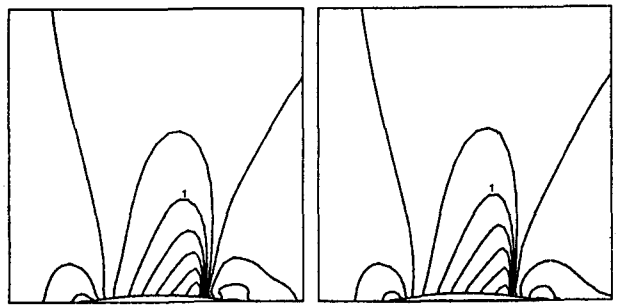

Fig.2a,b: Iso-Mach lines for Flux vector splitting and MUSCL (mesh 54X25)

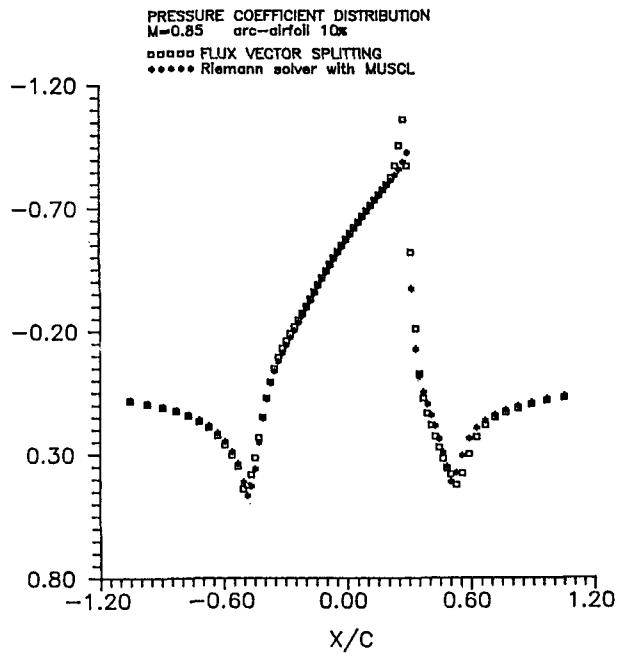

Fig.3: Comparison of the pressure coefficient distribution for the two methods,mesh (54X25)

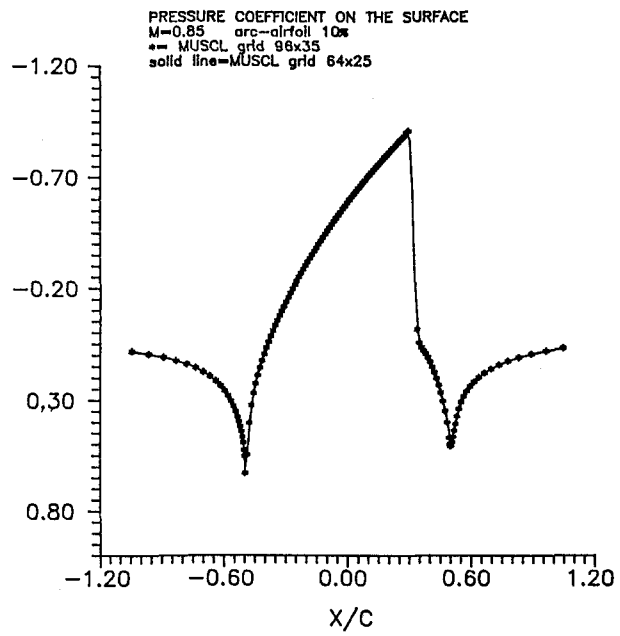

Fig.4: Comparison of the pressure coefficient distribution with MUSCL for two different meshes (64X25) and (96X35)

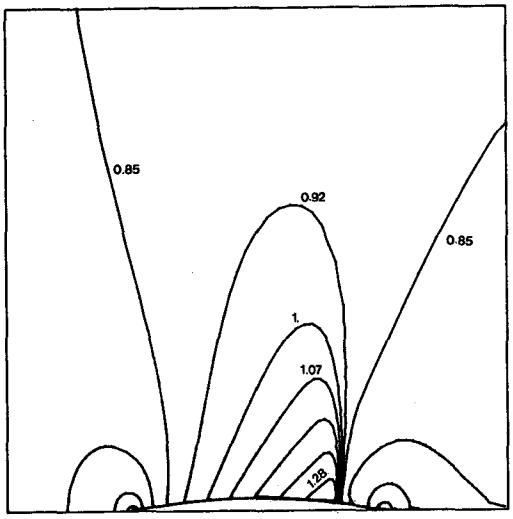

Fig.5: Iso-Mach lines for the finest mesh 96X35 Solution with the Riemann solver and MUSCL upwind

The mesh sequencing technique

The varying mesh sequencing technique is based on the use of sequence grids of coarseness[11][14]. In this method the coarser grid levels make an initial guess for the fine grid and act also as a treatment to the initial transient phase. The solution of the equations is obtained at first on a sequence of coarser meshes and then interpolating the solution up to the next finer grid. When the fine grid with mesh size h is given the choice of a coarse grid, with mesh size H, it is often straightforward. The coarse meshes are constructed discarding lines of the finer meshes in each direction. The coarsening ratio H/h=2 is usually optimal. It is the smallest recursivelly convenient number, and it is already big enough to make the coarse mesh computational work quite small relative to the finest mesh work. The use of the larger H/h ratio doesn't degrade any further the numerical convergence. In the computational code the coarser meshes and constructed as uniform meshes and act over the domain with no particular relation to the fine grid.Thus, a finite volume on the coarser mesh is constituted from, four cell volumes of the finer mesh. For inviscid flows the grid refinement on the coarser meshes isn't necessary nor is it for viscous flows if the finest mesh has been constructed with enough clustering of the mesh lines in regions with large gradients.

The construction of a typical coarse mesh is shown in figure (6a). Another way is to coarsen in terms of the cell taking every second cell of the fine mesh as a coarse cell. Then the coarse mesh values will be placed at coarse-cell positions analogous to their positioning on the fine cells.Thus the volumes of the corse mesh are a subset of the volumes of the fine mesh but the coarse grid points are not a subset of the correspondence on the fine grid. In our computational code the first procedure, (four cells of the fine grid gives one cell of the coarse grid) is implemented.

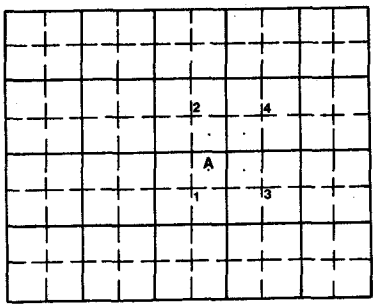

Fig.6a: Construction of a typical coarse mesh

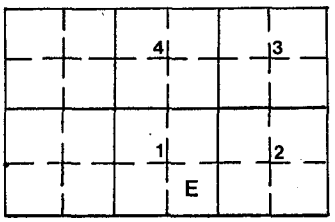

Fig.6b: Boundary cells on the mesh sequecing technique

The most sensitive part of the method is the interpolation procedure. The interpolation is obtained for each variable independently from the other. The values of the finer mesh can be obtained from a weighted average of the values of the coarser mesh. For example, the values of volume A (fig.6a) at the fine grid can be obtained as:

$$U_A = \frac{1}{16}\,(9U_1+3U_2+3U_3+U_4)$$

where 1,2,3,4 are volumes of the coarse mesh.

The transfer of the values can also be obtained by a rule which takes into account the cell area of the volumes. This rule has been used for the multigrid methods by other authors. Numerical experiments have shown that there is no difference in the effi-

ciency of the numerical convergence using the above two methods. Special treatment is given to the interpolation of the boundary points. Because the numerical method is a finite volume scheme, we need to find the values of the variables on the first cell over the boundary. Bilinear extrapolation is used for these volumes (fig.6b).

$$U_E = 0{,}9375\ U_1 - 0.1875\ U_4 + 0.3125\ U_2 - 0.0625\ U_3$$

The same technique can be used without changes for the solution either of the Navier-Stokes or the Euler equations. Another advantage of the mesh sequencing originates from the use of the relaxation procedure. As we mentioned in the previous paragraph some sub-iterations are needed for the relaxation method. In the coarse meshes the number of sub-iterations can be less than the correspondence number on the fine grid, because the convergence rates are better on the coarser meshes.

Local adaptive mesh solution

Presentation of the procedure

As it was mentioned in the previous paragraph, the numerical solution of the equations is not necessary in obtaining the whole flow field during the iterations. This fact originates from the nonuniformities of the flow variations towards a steady or an unsteady solution[12]. Thus, local iterations can be used in regions where the variations are large. This technique has been used in a simple form by Cline[13] in the VNAP code while an analytical study of the numerical disturbance was recently presented by Panaras,[12] for the case of thin-layer Navier-Stokes equations

Another fact, which is shown in the present work, is that the adaptation of the partial meshes can optimize the computational work.

For this reason prescribed convergence criteria can be defined in order to control the construction of the local meshes and the strategy of the solution during the numerical convergence. These convergence criteria can be physical or numerical. In the present paper numerical criteria are defined to terminate the calculations. These are the differences of the calculated conservative variables. On the other hand, the adaptation procedure implements the above criteria and also the convergence rates.

The adaptation of the local solution starts after the mesh sequencing technique when the numerical convergence meets one prescribed criterion. In this stage some partial meshes are constructed in different places of the flow field. Moreover, the method automatically defines the criterion for the new adaptation after some iterations. After each adaptation the equations are solved on the partial meshes. The values on the boundary cells of the partial meshes are calculated considering characteristic boundary conditions. Another way is to freeze the values around the partial meshes but the effect of the above implementation is in progress.

After the sufficient convergence of the partial meshes the solution can be repeated on the finest mesh. In this case the flow will be disturbed, but the convergence rates will be very fast, especially in the Navier-Stokes calculations. On the other hand, if the convergence rates after the converged local solution are bad, the adaptation can be repeated until the solution is achieved on the finest mesh by fast convergence rates.
This dependends upon the prescribed convergence rates on the finest mesh and upon the input adaptation levels.

The generation of the numerical disturbance and the application of the local adaptive mesh techique are also presented in the next paragraph for the inviscid and laminar viscous flow.

Results

Inviscid flow

The transonic (M=0.95) inviscid flow over a non lifting NACA 0012 airfoil has been studied using the above technique. The inviscid fluxes have been evaluated using the MUSCL type approach. The two coarser levels, used of both the Euler and the Navies-Stokes equations for the calculation, are presented in figures 7a, 7b and a partial view of the finest grid around the airfoil is shown in figure 7c.

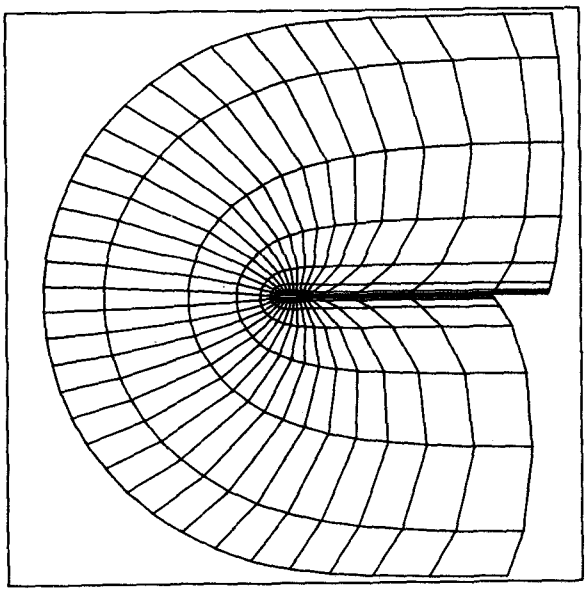

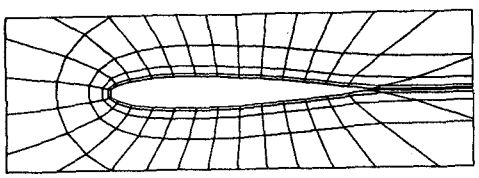

a

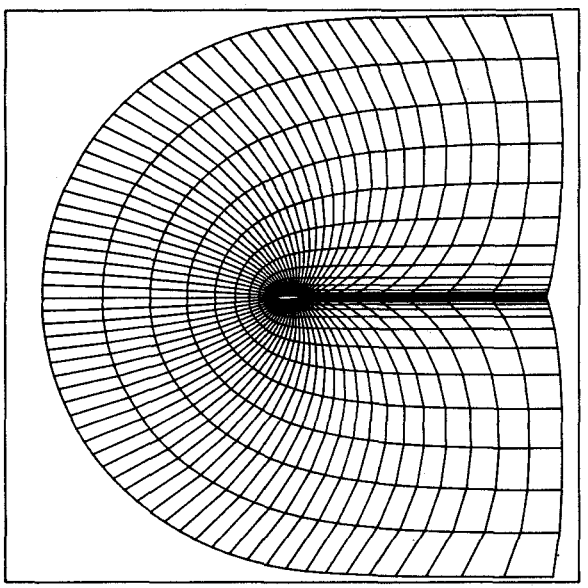

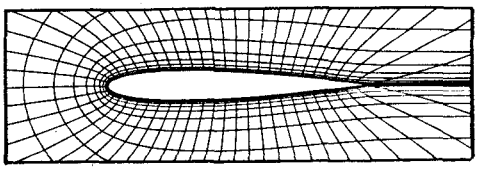

b

Fig.7a,b: Coarser meshes and partial view around the airfoil

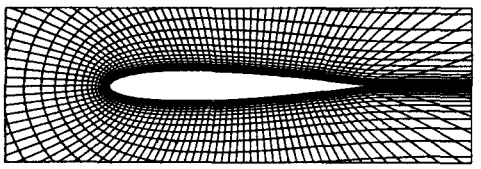

Fig.7c: Partial view of the finest mesh

The generation of the numerical disturbances are shown in figure 8. The propagation of the numerical disturbance is studied using the changes $\Delta(\rho u)$ and $\Delta(\rho w)$ of the conservative variables. The ΔQ_i (i=1,2 for ρu, ρw respectively) have been enlarged by a factor 10^4 - 10^6 for presentation in the plots.

Initially (Fig.8a) the disturbances are large in the whole flow field but especially in the regions where the two shock waves are generated. For this test case there is a shock wave in the trailing edge and a second in the wake region. For this figure the max ($\Sigma\Delta U_i$), (where ΔU_i are the changes of the four conservative variables), are $9X10^{-3}$. In figure 8b, where the above criterion is $1.3X10^{-3}$ the numerical disturbances are large only in the shock wave and the wake regions and only small disturbances are presented over the airfoil near the trailing edge. From this plot it is implied that the local solution can be applied now to these regions where the disturbances are large. In figure 8c the disturbances appear in the same regions but they are eliminated near the farfield boundary. The disappearance is stronger (fig. 8d) when the max ($\Sigma\Delta U_i$) is $1.2X10^{-4}$. During the above convergence the partial meshes are constructed by an adaptation method. Gradually the disturbances are completely eliminated (fig. 8e).

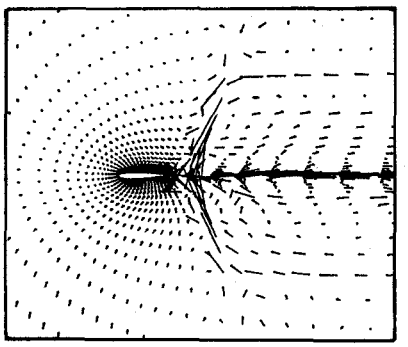

a

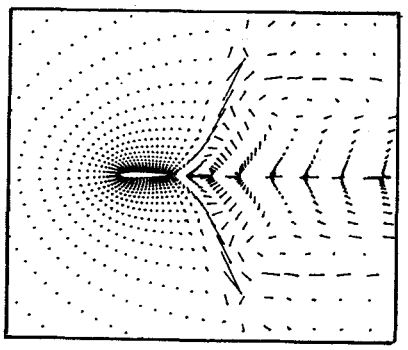

b

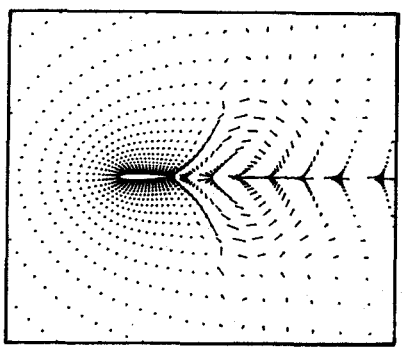

c

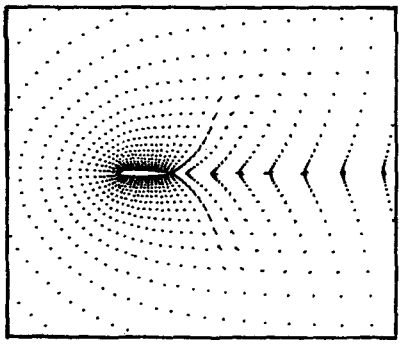

d

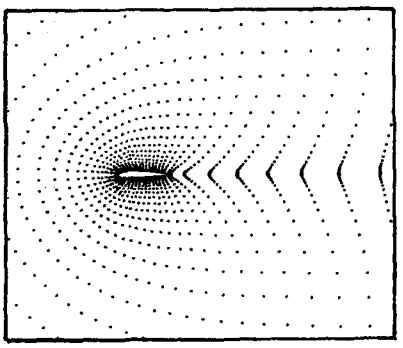

e

Fig.8a-e: Numerical disturbances for the inviscid transonic flow (M_∞=0.95, a=0)

For this test case the convergence histories of the max (ΔU_i) are presented in figure 9 for the case of the single grid, and for the cases of the mesh sequencing with and without local mesh solution. From this figure it is shown that with the local solution the convergence rates are faster than the mesh sequences only. The curve is almost vertical because the ratio of the number of cells on the partial meshes over the number of cells on the whole grid is very small and as a result the computational work units (1 work unit = 1 time step on the finest grid) are few. Because of the maximum change of the conservative variable on a single cell is plotted, instead of the mean one, oscillations are caused on the convergence history. These are observed on the trailing edge for the present test case.

In figure 10 the Mach number contours are shown for the inviscid test case (M_∞=0.95, a=0). An oblique shock wave is formed at the trailing edge and a second shock wave is observed on the wake region. The results have been compared with the correspondence results from the AGARD test cases [17]. Figures 11a and 11b indicate excellent agreement for the pressure coefficient and the Mach number distribution along the airfoil surface. In figure 12 the Mach number distribution behind the trailing edge indicates the secondary shock wave.

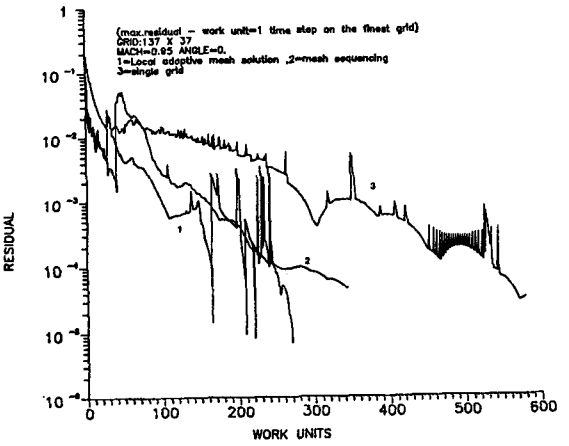

Fig.9: Convergence history for the inviscid transonic flow (M_∞=0.95, a=0)

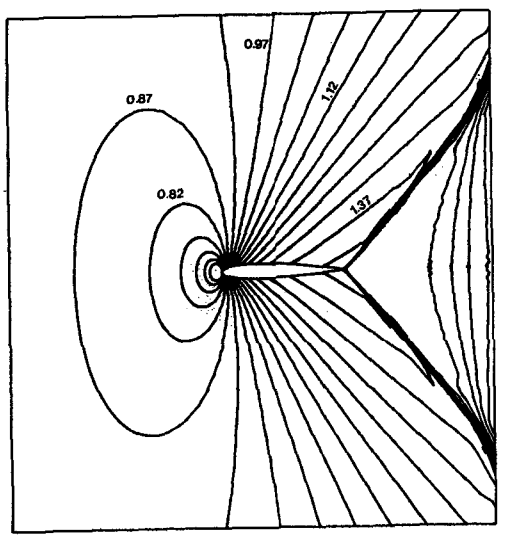

Fig. 10: Iso-Mach lines for the inviscid flow (M_∞=0.95, a=0)

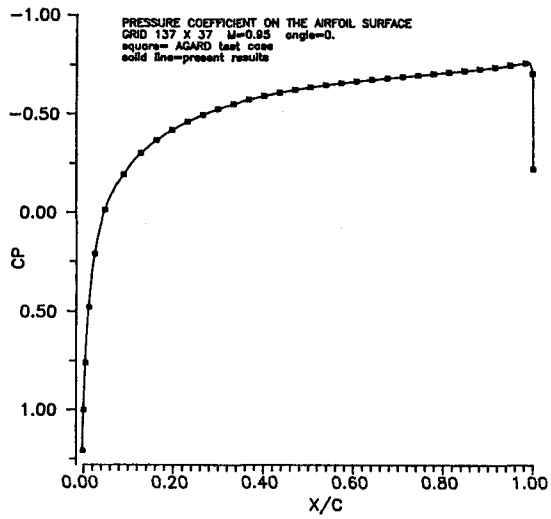

Fig.11a: Pressure coefficient distribution (M_∞=0.95, a=0)

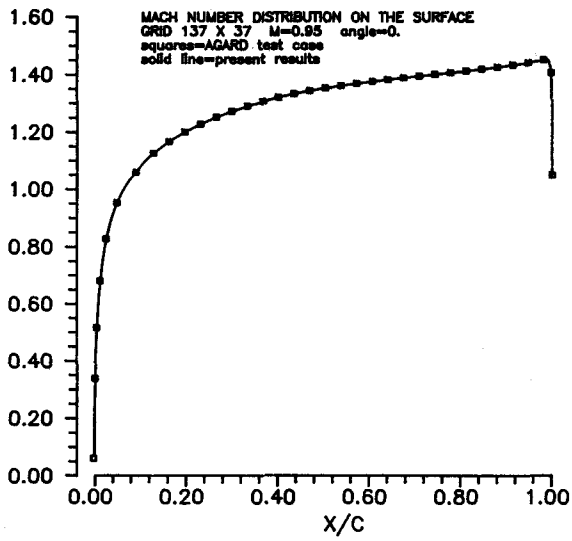

Fig.11b: Mach number distribution (M_∞=0.95, a=0)

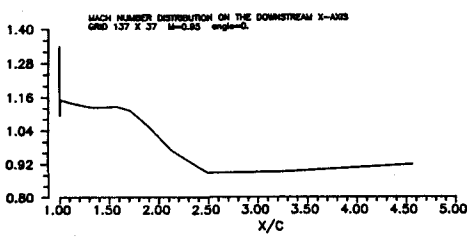

Fig.12: Mach number distribution on the downstream x-axis

Laminar viscous flows

The first test case is the supersonic laminar viscous flow (M_∞=2, a=10^o, R_e =106) over a NACA 0012 airfoil. The flow was calculated using a 137X37 mesh (108 points around the airfoil).

The outer boundary is located 9 chords from the airfoil and the first mesh line has a distance of 5.10^{-4} chords from the surface and the wake line. The grid around the airfoil is C-type and is generated by the Sorenson method [16]. Thus, we can control the spacing between the mesh lines from the boundary and the angles at which mesh lines inter sect the boundaries. A partial view of the mesh around the airfoil is shown in figure 7c.

The genaration of the disturbances are shown in figures 13a-e initially, the distrurbances are larger in the region of the bow shock, in the boundary layer and the wake of the flow field. After a number of iterations, the disturbances disappear from the region of the bow shock and propagation occurs on the downstream of the flow. On the upper side larger disturbances on the surface near the tailing edge are presented. This doesn't happen on the lower side. Thus, the adaptation procedure of the local solution takes into account a larger portion of the mesh on the upper plane than on the lower plane. Finally, the disturbances are limited to the wake region and die out when the convergence is achieved (figures 13d,e). In figures 14a-c some levels of the local solution are schematically shown. The iso-Mach lines are presented in figure 15a and the pressure coefficient distribution in figure 15b. The results are compared with the correspondent of the GAMM - workshop [18]. In figure 16 the convergence histories for this test case are plotted. As we can observe, the local solution improves the mesh sequencing technique and gives an important reduction of the computational time, compared with the single grid. After the repeated calculation on the finest grid the convergence rates are very fast. It is noted that no difference was apparent in the results after the calculation on the finest grid.

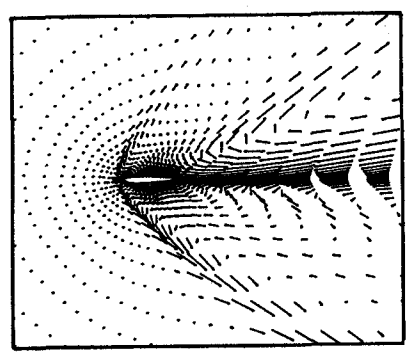

a

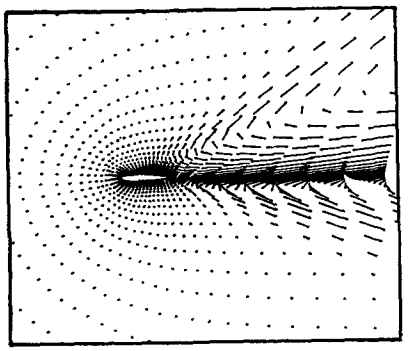

b

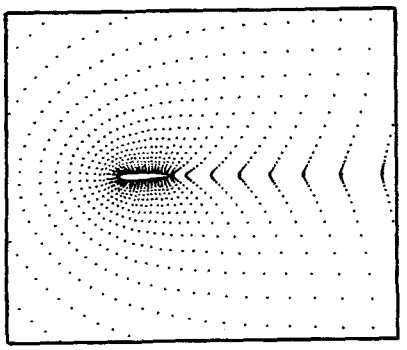

e

Fig.13a-e: Numerical disturbances for viscous laminar flow (M_∞=2, a=10, Re=106)

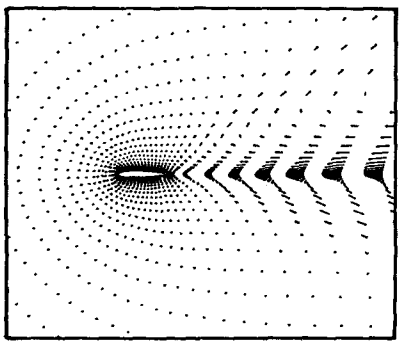

c

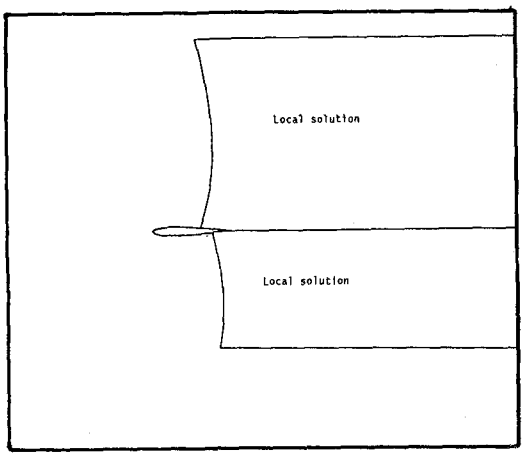

a

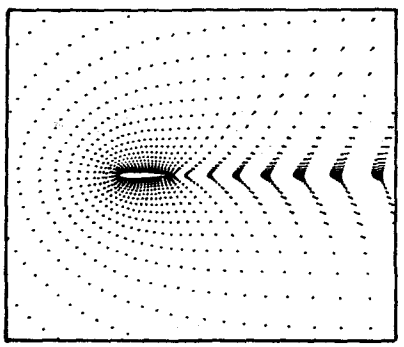

d

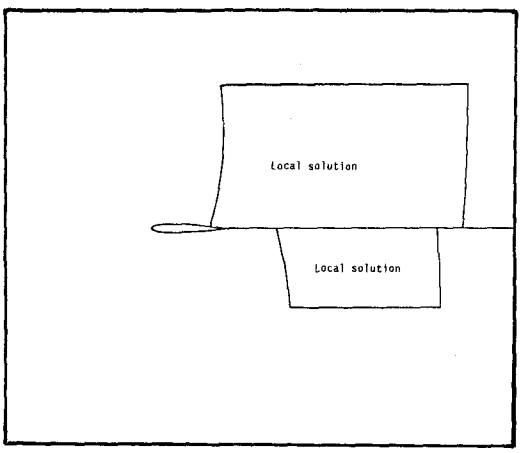

b

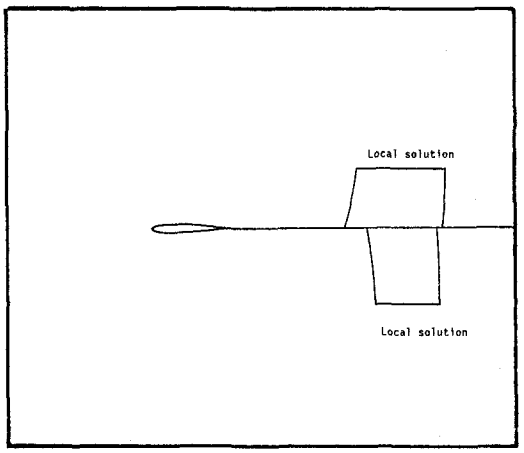

c

Fig.14a-c: Zones of the partial meshes for the local adaptive solution

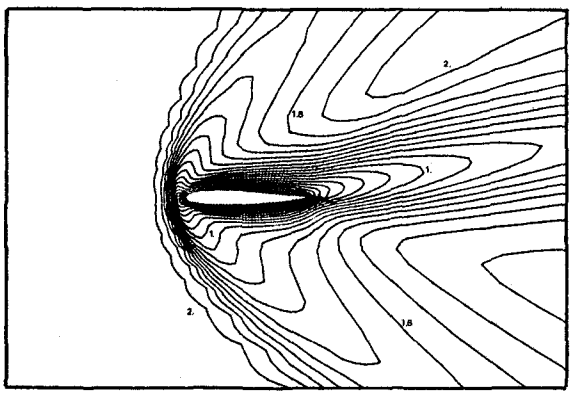

Fig.15a: Iso-Mach lines for M_∞=2, a=10, Re=106

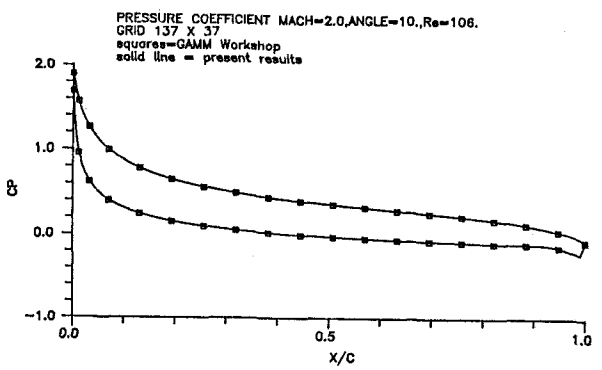

Fig.15b: Pressure coefficient distribution M_∞=2, a=10, Re=106

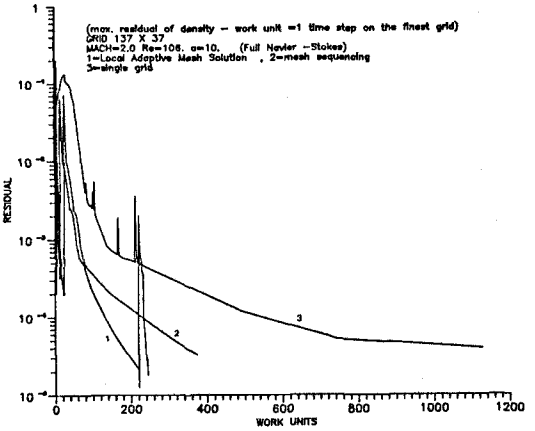

Fig.16: Convergence histories for viscous laminar flow

The last test case is the transonic laminar flow (M_∞=0.85, Re=500, a=0) over a NACA 0012. The iso-Mash lines are plotted in figure 17a and the pressure coefficient distribution in figure 17b. The behaviour of the convergences are similar with the previous test cases. The computational work with the local solution is small enough.

The local adaptive mesh solution doesn't increase the required computer storage. This is an important advantage for the solution of the Euler and Navier-Stokes equations on small computer systems.

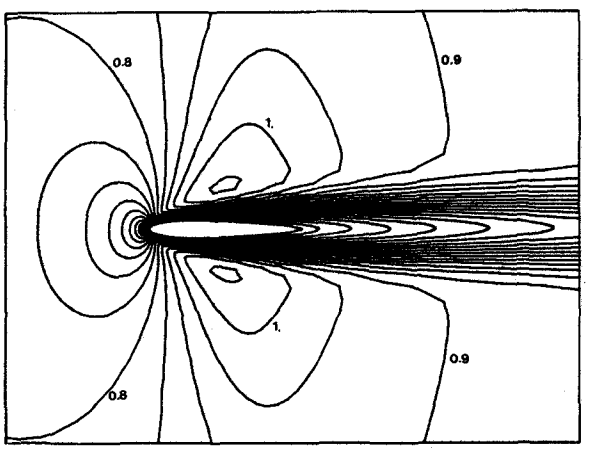

Fig.17a: Iso-Mach lines for M_∞=0.85, a=0,Re=500

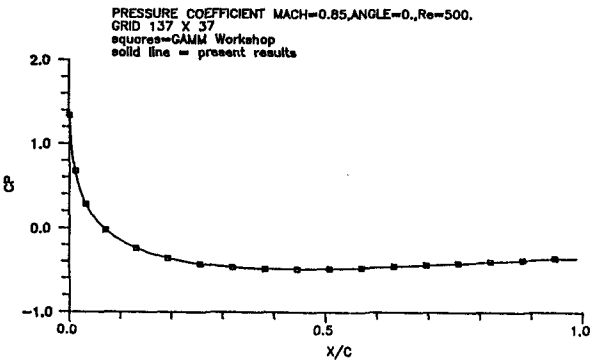

Fig17b: Pressure coefficient distribution (M_∞=0.85, a=0, Re=500)

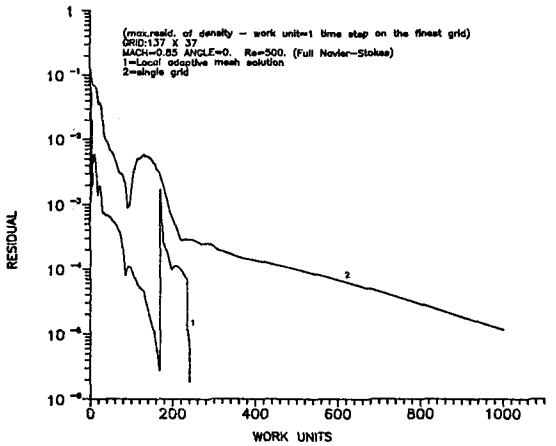

Fig. 18: Convergence history (M_∞=0.85, Re=500, a=0)

Conclusions

The MUSCL type approach can be used for the inviscid fluxes with very accurate results. The grid dependence proves that the MUSCL upwind, incorporated into the Riemann solver, can give accurate results even on coarser grids.

The solution of the Euler and Navier-Stokes equations can be obtained with smaller computational effort, using the local mesh solution. The local mesh solution improves the known mesh sequencing technique. The adaptation procedure constructs meshes with the minimum number of cells. On the other hand, further investigation of the adaptation criteria for the local solution is needed. The repeated solution on the finest mesh after the convergence on the partial meshes is not necessary. The above technique can be combined with other effective methods such as multigrid or adaptive grids. The computational gain is proportional to the finest mesh size. Therefore, in large scale calculations, such as the flow around a full aircraft or generally in three dimensional flows, the best efficiency is expected. In this paper results for the inviscid and laminar viscous flows are presented. The discretization of the viscous terms via the upwind scheme obtains accurate results for the present laminar flows.
The above methods will be expanded to turbulent flows after the introduction of a turbulence model. Furthermore a combination of the local adaptive mesh solution and the zonal approach is intended.

References

[1] Eberle, A. "3D Euler calculations using characteristic flux extrapolation", AIAA Paper 85-0119, 1985.

[2] Eberle, A., Schmatz, M.A., Schäfer, O., "High order solutions of the Euler equations by characteristic flux averaging," ICAS - Paper, 1.3.1, 1986.

[3] Schmatz, M.A., Brenneis, A., Eberle, A., "Verification of an implicit relaxation method for steady and unsteady viscous and inviscid flow problems", AGARD CP 437, pp 15-1 - 15-3.

[4] Schmatz, M.A., Hirschel, E.H., "Zonal solutions for airfoils using Euler, boundary layer and Navier-Stokes equations", In:Applications of computational Fluid Dynamics in aeronautics, AGARD CP 412, 1986.

[5] Chakravarthy, S.R., "The versatility and reliability of Euler solvers based on high accuracy TVD formulations", AIAA Paper 86-0243, 1986.

[6] Steger, J.L.,Warming , R.F., "Flux vector splitting of the inviscid Gasdynamic Equations with Application to Finite Difference Methods, "Journal of Computational Physics, Vol. 40, No 2, April 1981, pp. 263-293.

[7] Van Leer, B., "Towards the Ultimate Conservative Difference Scheme V.: A Second - Order Sequel to Godunov's Method, " Journal of Computational Physics, Vol. 32, 1979, pp. 101-136.

[8] Eberle, A., "Characteristic flux averaging approach to the solution of the Euler's equations", VKI Lecture Series, Computational Fluid Dynamics, 1987 -04, 1987.

[9] Chakravarthy, S.R., "High resolution Upwind formulations for the Navier-Stokes Equations, VKI Lecture Series, Computational Fluid Dynamics, 1988-05, 1988.

[10] Anderson, W.K., Thomas, J.L., Van Leer, B., "Comparison of Finite Volume Flux Vector Splittings for the Euler Equations, " AIAA Journal, Vol.24, Sept. 1986, pp. 1453-1460.

[11] Pulliam, T.H., Steger, J.L.,"Recent Improvements in Efficiency Accuracy and Convergence for implicit approximate factorisation algorithm" AIAA paper 85-0360, 1985.

[12] Panaras, A.G., "The Spatially Non-uniform Convergence of the Numerical Solutions of Flows", Journal of Computational Physics, Vol. 82, pp 429-453, 1989.

[13] Cline, M.C., Los Alamos National Laboratory Report LA -8872, 1981 (unpublished).

[14] Drikakis, D., Tsangaris. S., "Convergence Acceleration for a Finite Volume Scheme of the Euler Equations Using Mesh Sequencing, " 3rd International Congress of Fluid Mechanics, Cairo, January 2-4, 1990.

[15]Whitfield, D.L., Janus, J.M., "Three-Dimensional Unsteady Euler Equations Solution Using Flux Vector Splitting, "AIAA Paper, 84-1552, 1984.

[16]Sorenson, R.S., "A Computer program to generate two dimensional grids about airfoils and orther shapes by the use of Poisson's equation, "NASA TN-81198, 1981.

[17]"Test cases for inviscid flow field methods" AGARD Working Group 07, AR-211, 1985.

[18]Bristeau., M.D., Glowinski, R., Periaux, J.,Viviand, H., "Numerical Simulation of Compressible Navier-Stokes Flows, "Notes on Numerical Fluid Mechanics, Vol. 18, GAMM Workshop, Vieweg Verlag 1989.

Acknowledgement
We would like to thank Dr A.Panara for his helpful conversations on the subject of this work.